Phase Transformation and Metastability of Hygroscopic Microparticles

I. N. Tang, K. H. Fung, D. G. Imre, and H. R. Munkelwitz
Environmental Chemistry Division, Department of Applied Science, Brookhaven National Laboratory, Upton, New York 11973 U.S.A.

The hydration and crystallization of inorganic salt particles are investigated in an electrodynamic balance, in which a levitated single microparticle is undergoing phase transformation and growth under controlled humidity conditions. Laser Raman and Mie scattering techniques are used to probe the chemical and physical state of the microparticle before and after phase transformation. Here, we report first spectroscopic evidence that new metastable solid states form in hygroscopic aerosol particles. Because of the high degree of supersaturation at which a solution droplet solidifies, a metastable crystalline or amorphous state often results. The formation of such state is not predicted from bulk-phase thermodynamics and, in some cases, the resulting metastable state is entirely unknown heretofore. We also document new solid-solution and solid-solid phase transitions which occur exclusively in microparticles. Results are presented for particles composed of $(NH_4)_2SO_4$, Na_2SO_4, $LiClO_4$, $Sr(NO_3)_2$, $KHSO_4$, $RbHSO_4$ or NH_4HSO_4, illustrating the common occurrence of metastable states in hygroscopic aerosol particles under ambient conditions. It is also shown that certain thermodynamic properties can be determined with good precision from the vapor solid equilibrium during particle growth.

INTRODUCTION

Atmospheric aerosol particles are composed mostly of inorganic sulfates, nitrates, and/or chlorides, which are hygroscopic by nature and exhibit the properties of deliquescence and efflorescence in humid air. It is well known that, in addition to fog and cloud formation, ambient aerosols also play an important role in many other relevant atmospheric processes affecting the local air quality, visibility degradation, and the global climate as well. The hydration behavior, the oxidation and catalytic capabilities for trace gases, and the optical and radiative properties of the ambient aerosol, all depend crucially upon the chemical and physical states in which these microparticles exist. Indeed, the existence of hygroscopic aerosol particles as metastable aqueous droplets at high supersaturation, instead of being in their stable crystalline phases as might be expected from thermodynamic considerations, has routinely been observed in laboratories (Orr et al. 1958; Tang et al. 1977; Richardson and Spann 1984) and recently verified in the ambient atmosphere (Rood et al. 1989).

A deliquescent salt particle, such as $(NH_4)_2SO_4$, exhibits characteristic hydration behavior in humid air. A typical growth/evaporation cycle is illustrated in Fig. 1. Here, the particle mass change resulting from water vapor condensation (open circles) or evaporation (filled circles) is expressed as moles of water per mole of solute ($\#H_2O$/Solute) and plotted as a function of relative humidity (RH). Thus, as RH increases, a solid $(NH_4)_2SO_4$ particle remains unchanged (Curve A) until RH reaches 80%, when it deliquesces spontaneously (Curve B) to form a saturated solution droplet contain-

Aerosol Science and Technology 23:443–453 (1995)

Published by Elsevier Science Inc.

0278-6826/95/$9.50
SSDI 0278-6826(95)00026-C

ing about 8 #H_2O/Solute. The droplet continues to grow as RH further increases (Curve C). Upon evaporation, the solution droplet passes the deliquescence point without phase change and becomes highly supersaturated as a metastable droplet (Curve D). Finally, crystallization occurs at about 37% RH (Curve E). Note that, in a bulk solution, crystallization always takes place not far beyond the saturation point. This happens because the presence of dust particles and the container walls invariably induces heterogeneous nucleation at a much earlier stage than would homogeneous nucleation result in a solution droplet. The hysteresis loop shown in Fig. 1 represents a typical behavior exhibited by deliquescent aerosol particles. The observations reported by Rood et al. (1989) revealed that, at three urban and rural sites, the existence of metastable droplets indeed occurred more than 50% of the time when RH was between about 45% and 75%.

In this work, spectroscopic evidence of new solid metastable states in microparticles is presented for the first time. Because of the high supersaturation at which a solution droplet solidifies, a metastable state often results. The formation of such state is not predicted from bulk-phase thermodynamics and, in some cases, the resulting metastable states are entirely unknown heretofore. Observations are also reported on new solid-solution and solid-solid phase transitions which occur exclusively in microparticles. The results indicate that metastability is common in microparticles. Thus, the role of aerosols in atmospheric processes can not always be assessed solely on the basis of bulk-phase properties.

EXPERIMENTAL SECTION

In recent years, experimental methods developed for trapping a single micron-sized particle in a stable optical or electrical potential well have made it possible to study many physical and chemical properties of aerosol particles. These properties are either unique to small particles or

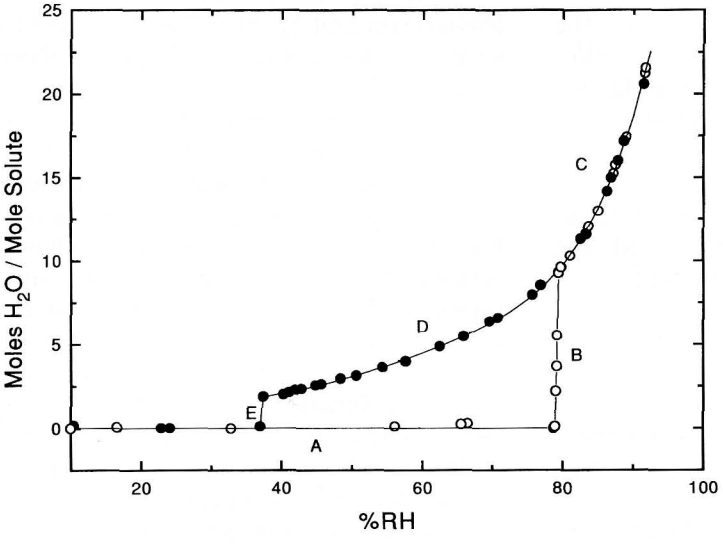

FIGURE 1. Hydration of an $(NH_4)_2SO_4$ particle, showing mass changes upon exposure to changing relative humidity at 25°C.

otherwise inaccessible to measurement with bulk samples. An earlier review by Davis (1983) documented the progress up to 1982. Since then, many interesting investigations have appeared in the literature. In particular, thermodynamic (Richardson and Kurtz 1984; Tang et al. 1986; Cohen et al. 1987) and optical properties (Tang and Munkelwitz 1991, 1994) of electrolyte solutions at concentrations far beyond saturation that could not have been achieved in the bulk, can now be measured with a suspended microdroplet. This is accomplished by continuously monitoring the changes in weight and in Mie scattering patterns of a single suspended solution droplet undergoing controlled growth and evaporation in a humidified atmosphere, thereby providing extensive data over the entire concentration region. Other interesting works on the physics and chemistry of microparticles have been covered in the recent review by Davis (1992). Experimental techniques have also been developed to characterize the physical and chemical state of suspended single microparticles by Raman spectroscopy (Fung and Tang 1988, 1989, 1991, 1992a, 1992b; Tang and Fung 1989; Davis et al. 1990; Buehler et al. 1991; Li et al. 1994; Fung et al. 1994). In this paper, the results of microparticle hydration studies, in conjunction with Raman spectroscopy for species identification, are presented.

Single particle levitation is achieved in an electrodynamic balance (or quadrupole cell) that has been described elsewhere (Fung and Tang 1989; Tang and Munkelwitz 1991). Briefly, an electrostatically charged particle, 14–16 μm in diameter, is trapped at the null point of the cell by an ac field imposed on a ring electrode surrounding the particle. The particle is balanced against gravity by a dc potential, U, established between two endcap electrodes positioned symmetrically above and below the particle. All electrode surfaces are hyperboloidal in shape and separated by Teflon insulators. When balanced at the null point, the particle mass, m, is given by

$$m = qU/gz_0, \tag{1}$$

where q is the number of electrostatic charges carried by the particle, g the gravitational constant, and z_0 the characteristic dimension of the cell. It follows that the relative mass changes, m/m_0, resulting from water vapor condensation or evaporation can be measured as precisely as measurement of the dc voltage changes, U/U_0, necessary for restoring the particle to the null point. Here, the subscript, 0, refers to measurements for the initial dry salt particle.

In particle hydration studies, a vertically polarized He–Ne laser is used to illuminate the particle. The particle position is continuously monitored by a CCD video camera and displayed on a TV screen for precise null point balance. The 90° scattered light is also continuously monitored with a photomultiplier tube. The laser beam, which is mechanically chopped at a fixed frequency, is focused on the particle so that a lock-in amplifier can be used to achieve high signal-to-noise ratios in the Mie scattering measurement. Data are routinely taken with a personal computer. Initially, a filtered solution of known composition is loaded in a particle gun; a charged particle is injected into the cell and captured in dry N_2 at the center of the cell by properly manipulating the ac and dc voltages applied to the electrodes. The system is closed and evacuated to a pressure below 10^{-7} torr. The vacuum is then valved off and the dc voltage required to position the particle at the null point is now noted as U_0. The system is then slowly back filled with water vapor during particle deliquescence and growth. Conversely, the system is gradually evacuated during droplet evaporation and efflorescence. The water vapor

pressure, p, and the balancing dc voltage, U, are simultaneously recorded in pairs during the entire experiment. Thus, the ratio, U_0/U, represents the solute mass fraction and the ratio, p/p^0, the corresponding water activity at that point. Here, p^0 is the vapor pressure of water at the system temperature. The measurement can be repeated several times with the same particle by simply raising the water vapor pressure again and repeating the cycle. The reproducibility is better than $\pm 2\%$.

A schematic diagram for Raman scattering studies is shown in Fig. 2. The same particle that is being levitated in the quadrupole cell for the hydration experiment is now excited by the 4880 Å line of an argon-ion laser (Coherent Innova-400). The polarization of the laser beam is set to be perpendicular to the scattering plane. A 10-cm focal length lens focuses the laser beam from the bottom of the cell onto the particle with about 500 mW power. The scattered light is collected with a condenser lens and is imaged onto the entrance slit of a double monochromator (SPEX 1403) with a resolution of 1.0 cm^{-1}. The light collecting optics are optimized at $f/1$ and is set to match the $f/7$ of the monochromator. The setting of the monochromator slit width is determined by the projected image size and the optimal resolution. The photon detection system is a cryogenically cooled CCD detector (SPEX Industries, NJ). The scattering background is further reduced by a holographic bandpass filter (Physical Optics Corp., CA). For a typical spectrum, the total exposure time of the detector is about 20 sec. Optical scattering spectra are transferred by a DMA interface board to the 486-based computer and stored on floppy disks for later data analysis. The monochromator is routinely calibrated against the neon spectrum. As a result, the accuracy of the monochromator is about 0.1 cm^{-1}. However, the practical resolution of the spectrometer is typically 0.5 cm^{-1}, owing to an increase in the slit width needed to accommodate the projected particle image size.

RESULTS AND DISCUSSION

Experimental observations are presented here for four different salt systems, namely, Na_2SO_4, $LiClO_4$, $Sr(NO_3)_2$, and the bisulfates. The results illustrate the various phase transformations and metastable states that hygroscopic particles may undertake under humid conditions expected in the ambient atmosphere.

(1) *Na_2SO_4 Particles.* In bulk solutions at temperatures below 35°C, sodium sulfate crystallizes with ten water molecules to form the stable solid phase decahydrate, $Na_2SO_4 \cdot 10H_2O$ (Seidell and Linke 1965). In suspended microparticles, however, it is the anhydrous solid, Na_2SO_4, that is formed most frequently from the crystallization of supersaturated solution droplets. This fact is established both by particle mass measurements and by Raman spectroscopy. The Raman shifts for the anhydrous solid and the decahydrate occur at 992 and 995 cm^{-1}, respectively, which can be identified unambiguously with the Raman spectrometer.

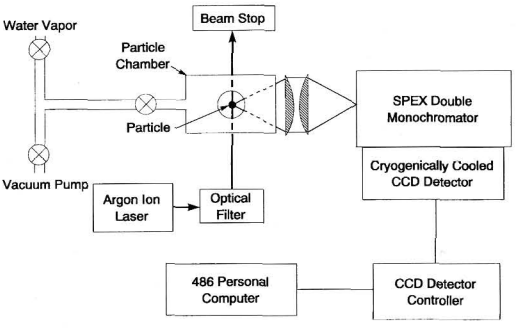

FIGURE 2. Schematic diagram of the experimental setup for single particle Raman spectroscopy.

Figure 3 shows the growth (open circles) and evaporation (filled circles) of a Na_2SO_4 particle in a humid environment at 25°C. The hydration behavior is qualitatively very similar to that of the $(NH_4)_2SO_4$ particle shown in Fig. 1. Thus, as RH increases, an anhydrous Na_2SO_4 particle deliquesces at 84% RH to form a saturated solution droplet containing about 13 $\#H_2O$/Solute. Upon evaporation, the solution droplet becomes highly supersaturated until, finally, crystallization occurs at about 58% RH. As mentioned earlier, in a bulk solution, crystallization takes place not far beyond the saturation point and the resulting crystalline form is the stable decahydrate, $Na_2SO_4 \cdot 10H_2O$.

However, since a suspended droplet remains in the metastable state to high levels of supersaturation where decahydrate is no longer the most stable state, the resulting solid particle is consistently the crystalline anhydrous Na_2SO_4. The relative stability between the anhydrous Na_2SO_4 and the decahydrate can be estimated from a consideration of the standard Gibb's free energy change, ΔG^0, the system:

$$Na_2SO_4(c) + 10H_2O(g) = Na_2SO_4 \cdot 10H_2O(c),$$

so that,

$$\Delta G^0 = \Delta G_f^0[Na_2SO_4 \cdot 10H_2O] - \Delta G_f^0[Na_2SO_4] - 10\,\Delta G_f^0[H_2O] = -RT\ln(1/p^{10}). \quad (2)$$

Here, c and g in the parentheses refer to the crystalline state and gas phase, respectively, R is the gas constant, and T is the absolute temperature. ΔG^0 may be evaluated from the tabulated values of standard free energy of formation, ΔG_f^0. Talking the tabulated (Wagman et al. 1981) ΔG_f^0 values -871.76, -303.59, and -54.635 kcal/mol for $Na_2SO_4 \cdot 10H_2O(c)$, $Na_2SO_4(c)$ and $H_2O(g)$, respectively, we obtain a value of -21.81 kcal/mol for ΔG^0, which leads to 19.2 torr as the equilibrium partial pressure of water vapor, p, according to Eq. 2, or

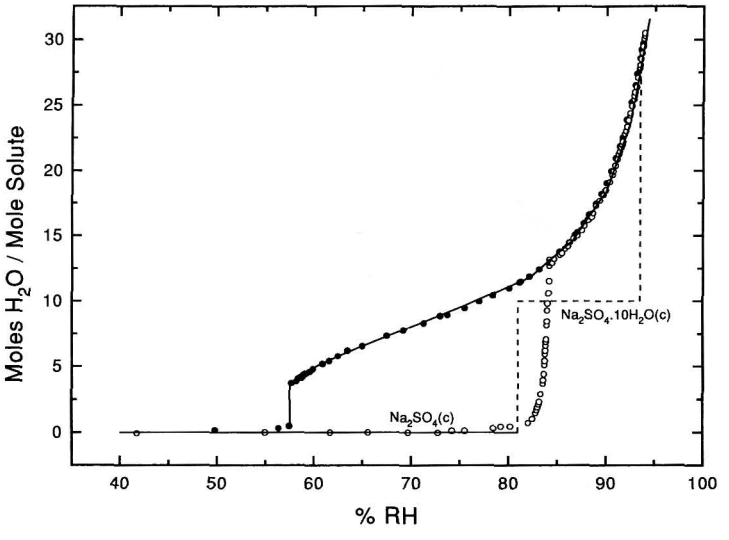

FIGURE 3. Hydration of a Na_2SO_4 particle in humid environment at 25°C.

81% RH at 25°C. It follows that, instead of decahydrate, the anhydrous Na_2SO_4 becomes the most stable state below 81% RH. Thus, as depicted by the dashed lines shown in Fig. 3, a solid anhydrous Na_2SO_4 particle would have transformed into a crystalline decahydrate particle at 81% RH, which would then deliquesce, according to solution thermodynamics (Goldberg 1981), at 93.6% RH to become a saturated solution droplet containing about 28 $\#H_2O$/Solute. The observed hydration behavior of the particle, as shown in Fig. 3, is quite different from what is predicted from the bulk-phase thermodynamics.

(2) *$LiClO_4$ Particles*. Solid-solid phase transitions do take place in $LiClO_4$ particles undergoing hydration in a humid environment. Figure 4 shows the growth (open circles) and evaporation (filled circles) of a $LiClO_4$ particle. The inset is an enlarged view of the low RH region. It shows that the growth curve follows the bulk-phase thermodynamics, predicting transformation to occur from $LiClO_4(c)$ to $LiClO_4 \cdot H_2O(c)$, and again to $LiClO_4 \cdot 3H_2O(c)$. The crystalline trihydrate particle subsequently deliquesces and becomes a solution droplet. The observed RH for the solid-solid phase transitions and solid-liquid deliquescence are 0.3%, 8.6%, and 67%, respectively. On the contrary, the evaporation path yields metastable phases. First, the solution droplet becomes highly supersaturated and crystallizes into a $LiClO_4 \cdot 3H_2O$ particle at ~ 40% RH. Next, the trihydrate particle becomes metastable from 8.6% down to ~ 1% RH, and then transforms into a monohydrate particle. Finally, the monohydrate particle remains metastable from 0.3% RH down and transforms into an anhydrous particle at ~ 0.03% RH.

It is interesting to note that, because of the metastable nature, some $LiClO_4$ particles during evaporation were observed to remain as supersaturated solution droplets to below 5% RH, at which point their water content was below the 1:3 ratio required in the trihydrate. Consequently, they crystallized directly into monohydrate, which was the stable form expected at the RH of their transition.

Because of the fact that in this work

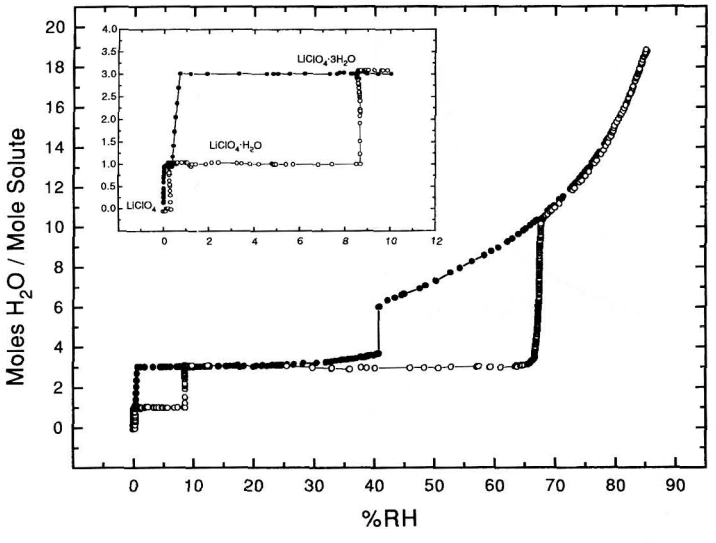

FIGURE 4. Hydration of a $LiClO_4$ particle in humid Environment at 25°C.

the transition pressures can be measured with good precision, the solid-vapor equilibria observed at the solid–solid phase transitions during particle growth offer a precise measurement of the standard free energies of formation for the solids. Thus, the standard free energy change, ΔG^0, for the reaction,

$$LiClO_4(c) + H_2O(g) = LiClO_4 \cdot H_2O(c),$$

is given by

$$\Delta G^0 = \Delta G_f^0[LiClO_4 \cdot H_2O] - \Delta G_f^0[LiClO_4] - \Delta G_f^0[H_2O] = -RT \ln(1/p). \quad (3)$$

Similarly, for the reaction,

$$LiClO_4 \cdot H_2O(c) + 2H_2O(g) = LiClO_4 \cdot 3H_2O(c),$$

we have

$$\Delta G^0 = \Delta G_f^0[LiClO_4 \cdot 3H_2O] - \Delta G_f^0[LiClO_4 \cdot H_2O] - 2\Delta G_f^0[H_2O] = -RT \ln(1/p^2). \quad (4)$$

The tabulated (Wagman et al. 1981) ΔG_f^0 values for $H_2O(g)$ and $LiClO_4 \cdot 3H_2O(c)$ are, respectively, -54.635 and -239.30 kcal/mol. The water vapor pressures measured at the anhydrous–monohydrate and monohydrate–trihydrate transitions are, respectively, 0.065 and 2.05 torr. Substituting the appropriate values into Eqs. 3 and 4, we obtain -123.02 and -62.84 kcal/mol as the ΔG_f^0 values for $LiClO_4 \cdot H_2O(c)$ and $LiClO_4(c)$, respectively. The tabulated (Wagman et al. 1981) ΔG_f^0 for the monohydrate is -121.8 kcal/mol, which agrees reasonably well with our value. No value is known for the anhydrous state, making our value the only measured ΔG_f^0 for $LiClO_4(c)$.

(3) *$Sr(NO_3)_2$ Particles.* Another interesting example is provided by the hydration behavior of $Sr(NO_3)_2$ particles. According to the solution thermodynamics (Seidell and Linke 1965), the equilibrium solid phase at room temperature is the tetrahydrate, $Sr(NO_3)_2 \cdot 4H_2O$. At 29.3°C and above, the anhydrous $Sr(NO_3)_2$ becomes the stable solid phase. The Raman spectra of the two solid phases are shown in Figs. 5a and 5b, respectively. Although the nitrate ion $\nu_1(A_1')$ symmetric stretch bands in the 1055–1058 cm^{-1} region show only a small difference between the two solid phases, their $\nu_4(E')$ deformation bands in the 722–748 cm^{-1} region are distinctively different due to hydrate formation. In dilute solutions, the solvated NO_3^- ion has broad Raman lines at 1048 and 718 cm^{-1}. With increasing solute concentrations, the 1048-cm^{-1} line gradually shifts to 1051 cm^{-1} and a shoulder at 734 cm^{-1}, which is assigned (Bulmer et al.

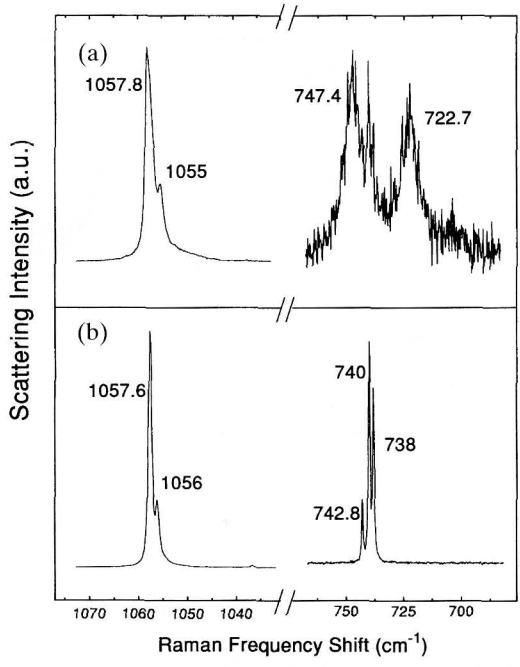

FIGURE 5. Raman spectra of solid strontium nitrate: (a) bulk tetrahydrate crystals, (b) bulk anhydrous crystals.

1975) to the NO_3^- ion bound to Sr^{++}, becomes more distinct. The spectra of a solution droplet shown in Fig. 6a reveal the saline features just described for concentrated solutions. However, it was observed that the droplet spectra Fig. 6a consistently turned into a spectra Fig. 6b at low RH. The new 1053-cm^{-1} line is as broad as the 1051-cm^{-1} line of the supersaturated solution droplet. In addition, while the 718-cm^{-1} line, which is normally attributed to the solvated NO_3^- ion, disappears completely, the 734-cm^{-1} line, which is assigned to nitrate ion bound to Sr^{++}, has shifted to 736 cm^{-1} and become quite pronounced. It was first (Fung and Tang 1992b) thought that the observed new spectra resulted from strongly bound ion pairs in highly concentrated $Sr(NO_3)_2$ solutions.

Subsequent Mie scattering experiments performed on the particle, however, indicated that the particle was not a spherical droplet, since the polarization of the elastically scattered light was randomized indeed. A study of the hydration behavior further revealed that the particle was, in fact, a metastable solid particle, which tended to retain water strongly even in vacuum. Upon increasing RH, the particle slightly but continuously absorbed water until it deliquesced distinctively at 69% RH, as clearly shown in Fig. 7b. Once in solution, the particle behaved like a typical solution droplet and solidified again at 60% RH upon evaporation. Judging from its broad Raman band at 1053 cm^{-1} and its hydration behavior, the metastable particle is likely an amorphous solid solution, which so far is not known to exist in bulk samples. A recent study (Chahti et al. 1990) of the undercooling of aqueous $Sr(NO_3)_2$ emulsions dispersed in oil has

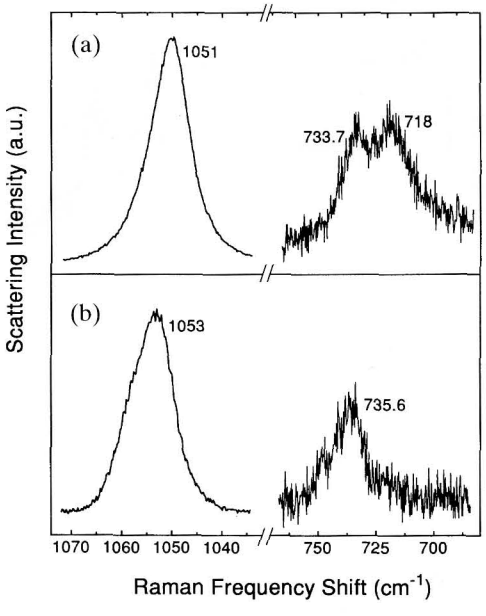

FIGURE 6. Raman spectra of strontium nitrate in different states: (a) a supersaturated solution droplet, (b) a metastable amorphous solid particle.

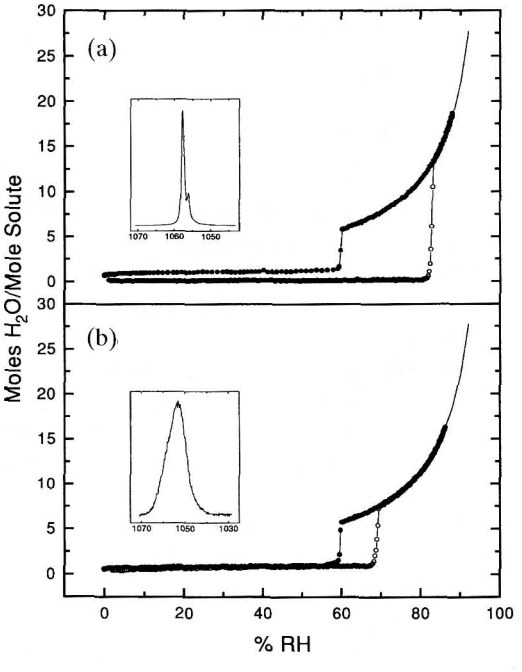

FIGURE 7. Hydration of $Sr(NO_3)_2$ particles: (a) a crystalline anhydrous solid, (b) a metastable amorphous solid.

also detected the existence of a metastable solid phase as evidenced by differential scanning calorimetry. However, neither spectroscopic nor hydration information is available from the previous study for a comparison with the present findings.

Once in a while, an amorphous solid particle was observed to transform abruptly and irreversibly into a crystalline anhydrous particle, which then deliquesced at 83% RH, as shown in Fig. 7a. The two insets in Fig. 7 display the Raman spectra of the particle in its different solid states before deliquescence. So far, no anhydrous particle, amorphous or crystalline, has been observed to transform into a solid tetrahydrate particle, which, if existed, would have deliquesced at 85% RH, according to solution thermodynamics (Seidell and Linke 1965).

(4) *Bisulfate particles*. Raman spectroscopic studies of suspended bisulfate particles further indicate the frequent formation of new solid metastable states in microparticles. Bulk-phase crystalline bisulfates such as NH_4HSO_4, $KHSO_4$, and $RbHSO_4$ have been the subject of several Raman (Arthur et al. 1974; Goypiron et al. 1980; Toupry et al. 1981) and x-ay diffraction (Nelmes 1971; Payan and Haser 1976) studies for their structure determination. These are interesting crystalline compounds, which undergo a second-order phase transition (Pepinsky et al. 1958) from a paraelectric to a ferroelectric phase at certain temperatures specific to each compounds. NH_4HSO_4, being a major component of acidic atmospheric aerosols (Brosset et al. 1975), is of particular importance because of its chemical reactivity and hygroscopic and optical properties.

Figure 8 shows a comparison of the Raman spectra between a suspended $KHSO_4$ microparticle and its bulk crystals. Because of hydrogen bonding, bulk-phase crystalline $KHSO_4$ is comprised of two distinct HSO_4^- groups (Payan and Haser 1976) in the asymmetric unit: one group forms dimers across a symmetry center, the other is linked into infinite chains along a glide plane. The splitting of the $\nu_3(A_1)$ symmetric stretch at lines 1027 and 1002 cm^{-1} are assigned (Dey et al. 1982) to dimers and chains, respectively. In a particle, however, the observed spectral lines are fewer, with only one predominant line at 1028 cm^{-1} remaining for the symmetric stretch mode. The structure of the particle is clearly new and quite different from that of the bulk phase. It is likely that, due to kinetic constraints, only one HSO_4^- group, possibly the dimers according to symmetry considerations, emerges to form the new crystalline phase from the highly supersaturated solution droplet.

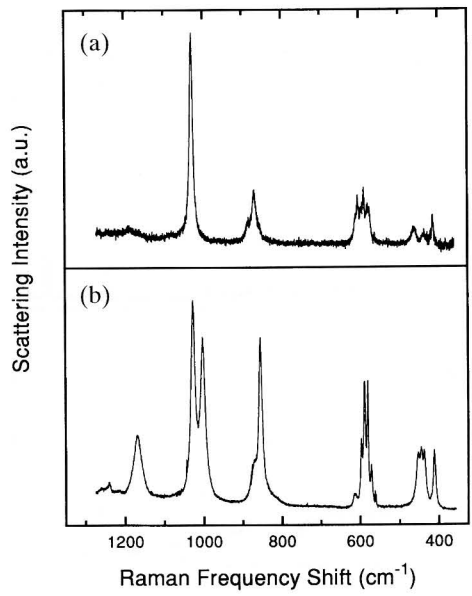

FIGURE 8. Raman spectra of $KHSO_4$: (a) a metastable particle, (b) bulk crystals.

Figures 9 and 10 display the Raman spectra of $RbHSO_4$ and NH_4HSO_4, respectively. While the individual Raman shifts are different in different systems, the general features between a particle

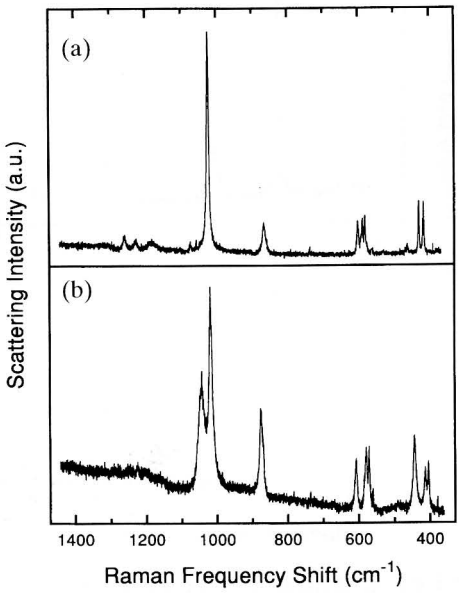

FIGURE 9. Raman spectra of $RbHSO_4$: (a) a metastable particle, (b) bulk crystals.

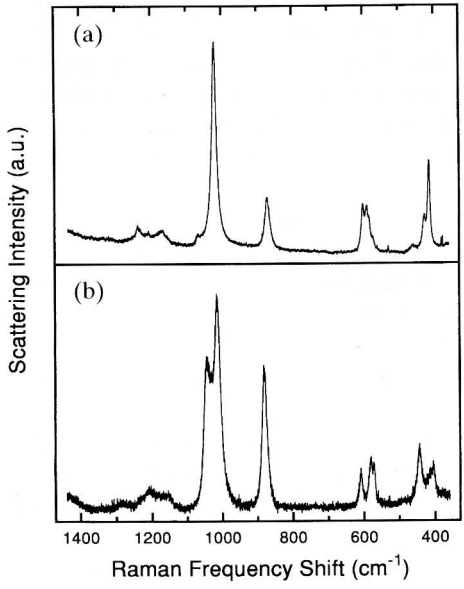

FIGURE 10. Raman spectra of NH_4HSO_4: (a) a metastable particle, (b) bulk crystals.

and the bulk phase are similar to those exhibited by $KHSO_4$. The stability of the new particle phases may also be different in different systems. $KHSO_4$ droplets crystallize exclusively in this new form and remain so indefinitely, whereas NH_4HSO_4 particles are alternately produced in either of the two analogous forms. The new form of NH_4HSO_4 is often observed to transform spontaneously and irreversibly into that of the bulk crystal under laser illumination, indicating that the new form is indeed a metastable state. It is also interesting to note that the two NH_4HSO_4 crystalline forms have different deliquescence points as well, namely, 37% and 40% RH for the metastable and equilibrium states, respectively.

CONCLUSIONS

Solid microparticles formed from supersaturated solution droplets are shown to be comprised of new metastable phases, which either are not predicted from the bulk-phase thermodynamics or have never been observed before. The chemical reactivity and hygroscopic properties of the metastable states may or may not be the same as what are known from studies of the bulk phase alone. Since ambient aerosol particles, including high altitude clouds, are all subjected to hydration and thermal cycles leading to the possible formation of metastable states, their physical and chemical properties need to be ascertained in order to fully assess their potential role in atmospheric chemistry. Indeed, Worsnop et al. (1994) have presented evidence that transient and metastable hydrates of nitric acid form by cooling liquid H_2SO_4 in the presence of stratospheric concentrations of HNO_3 and H_2O vapor. It is also plausible that, for some chemical systems not yet investigated, microparticles composed of metastable states may be produced that have certain desirable properties not found in the bulk phase.

Further studies may prove to be quite interesting.

This research was performed under the auspices of the U.S. Department of Energy under Contract No. DE-AC02-76CH00016.

REFERENCES

Arthur, J. W., Lockwood, D. J., and Taylor, W. (1974). *Adv.* Raman Spec. 1:144.

Brosset, C., Andreasson, K., and Ferm, M. (1975). *Atmos. Envir.* 9:631.

Buehler, M. F., Allen, T. M., and Davis, E. J. (1991). *J. Colloid Interface Sci.* 146:79.

Bulmer, J. T., Chang, T. G., Gleeson, P. J., and Irish, D. E. (1975). *J. Solution Chem.* 4:969.

Chahti, A., Carrier, P., and Dumas, J. P. (1990). *Phase Transitions* 27:203.

Cohn, M. D., Flagan, R. C., and Seinfeld, J. H. (1987). *J. Phys. Chem.* 91:4563.

Davis, E. J., *Aerosol Sci. Technol.* (1983). 2, 121; (1992). *Adv. Chem. Eng.* 18:1.

Davis, E. J., Buehler, M. F., and Ward, T. L. (1990). *Rev. Sci. Instrum.* 61, 1281.

Dey, B., Jian, Y. S., and Verma, A. L. (1982). *J. Raman Spec.* 13:209.

Fung, K. H., Imre, D. G., and Tang, I. N. (1994). *J. Aerosol Sci.* 25:479.

Fung, K. H., and Tang, I. N. (1988). *Appl. Opt.* 27:206; (1989), *J. Colloid Interface Sci.* 130:219; (1991), *Appl. Spectros.* 45:734; (1992a), 46:159; (1992b), 46:1189.

Goldberg, R. N. (1981). *J. Phys. Chem. Ref. Data* 10:671.

Goypiron, A., de Villepin, J., and Novak, A. (1980). *J. Raman Spec.* 9:297.

Li, W., Rassat, S. D., Foss, W. R., and Davis, E. J. (1994). *J. Colloid Interface Sci.* 162:267.

Nelmes, R. J. (1971). *Acta Cryst.* B27:272.

Orr, C., Hurd, F. K., and Corbett, W. J. (1958). *J. Colloid Sci.* 13:472.

Payan, F., and Haser, R. (1976). *Acta Cryst.* B32:1875.

Pepinsky, R., Vedam, K., Hoshino, S., and Okaya, Y. (1958). *Phys. Rev.* 111:1508.

Richardson, C. B., and Kurtz, C. A. (1984). *J. Am. Chem. Soc.* 106:6615.

Richardson, C. B., and Spann, J. F. (1984). *J. Aerosol Sci.* 15:563.

Rood, M. J., Shaw, M. A., Larson, T. V., and Covert, D. S. (1989). *Nature* 337:537.

Seidell, A., and Linke, W. F. (1965). *Solubilities of Inorganic and Metal Organic Compounds*, 4th ed. American Chemical Society, Washington, D.C.

Tang, I. N., and Fung, K. H. (1989). *J. Aerosol Sci.* 20:609.

Tang, I. N, and Munkelwitz, H. R. (1994). *Aerosol Sci. Technol.* 15:201; (1994), *J. Geophys. Res.* 99:18,801.

Tang, I. N., Munkelwitz, H. R., and Davis, J. G. (1977) *J. Aerosol Sci.* 8:149.

Tang, I. N., Munkelwitz, H. R., and Wang, N. (1986). *J. Colloid Interface Sci.* 114:409.

Toupry, N., Poulet, H., and Le Postollec, M. (1981). *J. Raman Spec.* 11:81.

Wagman, D. D., Evans, W. H., Parker, V. B., Schumm, R. H., and Nuttall, R. L. (1981). *Selected Values of Chemical Thermodynamic Properties*, NBS Technical Note 270-8, U.S. Department of Commerce.

Worsnop, D. R., Zahniser, M. S., Fox, L. E., and Wofsy, S. C. (1994). Presented at the 4th International Aerosol Conference, August 29–September 2, Los Angeles, California.

Received November 29, 1994; revised February 24, 1995